AGU PUBLICATIONS

JGR

Journal of Geophysical Research: Solid Earth

RESEARCH ARTICLE
10.1002/2013JB010928

Key Points:
- GIA dominates isostatic land motion along the U.S. Gulf Coast today
- Sediment load induced subsidence is <0.5 mm/yr in the Mississippi Delta
- The effective elastic thickness of the lithosphere is time dependent

Supporting Information:
- Readme
- Table S1

Correspondence to:
Z. Shen,
zshen@tulane.edu

Citation:
Wolstencroft, M., Z. Shen, T. E. Törnqvist, G. A. Milne, and M. Kulp (2014), Understanding subsidence in the Mississippi Delta region due to sediment, ice, and ocean loading: Insights from geophysical modeling, *J. Geophys. Res. Solid Earth*, *119*, 3838–3856, doi:10.1002/2013JB010928.

Received 23 DEC 2013
Accepted 31 MAR 2014
Accepted article online 3 APR 2014
Published online 28 APR 2014

Understanding subsidence in the Mississippi Delta region due to sediment, ice, and ocean loading: Insights from geophysical modeling

Martin Wolstencroft[1], Zhixiong Shen[2], Torbjörn E. Törnqvist[2], Glenn A. Milne[1], and Mark Kulp[3]

[1]Department of Earth Sciences, University of Ottawa, Ottawa, Ontario, Canada, [2]Department of Earth and Environmental Sciences, Tulane University, New Orleans, Louisiana, USA, [3]Department of Earth and Environmental Sciences, University of New Orleans, New Orleans, Louisiana, USA

Abstract The processes responsible for land surface subsidence in the Mississippi Delta (MD) have been vigorously debated. Numerous studies have postulated a dominant role for isostatic subsidence associated with sediment loading. Previous computational modeling of present-day vertical land motion has been carried out in order to understand geodetic data. While the magnitudes of these measured rates have been reproduced, the model parameter values required have often been extreme and, in some cases, unrealistic. In contrast, subsidence rates in the MD on the 10^3 year timescale due to delta loading estimated from relative sea level reconstructions are an order of magnitude lower. In an attempt to resolve this conflict, a sensitivity analysis was carried out using a spherically symmetric viscoelastic solid Earth deformation model with sediment, ice, and ocean load histories. The model results were compared with geologic and geodetic observations that provide a record of vertical land motion over three distinctly different timescales (past 80 kyr, past 7 kyr, and past ~15 years). It was found that glacial isostatic adjustment is likely to be the dominant contributor to vertical motion of the Pleistocene and underlying basement. Present-day basement subsidence rates solely due to sediment loading are found to be less than ~0.5 mm yr^{-1}. The analysis supports previous suggestions in the literature that Earth rheology parameters are time dependent. Specifically, the effective elastic thickness of the lithosphere may be <50 km on a 10^5 year timescale, but closer to 100 km over 10^3 to 10^4 year timescales.

1. Introduction

The Mississippi Delta (MD) and the adjacent U.S. Gulf Coast host a significant population, extensive economic activity, and critical ecosystem goods and services. The characteristic rate of twentieth-century relative sea level (RSL) rise in the MD is ~10 mm yr^{-1} [e.g., *Penland and Ramsey*, 1990], a value that contains both land subsidence and the sea-level changes caused by climate change (i.e., land ice melting and ocean warming). As a result, the MD region is particularly vulnerable to catastrophic events (e.g., storm surges associated with hurricanes) as well as more chronic environmental degradation, such as wetland loss from a range of largely human influences [*Day et al.*, 2007]. Reaching an understanding of land surface lowering involves identifying the relative contribution of basement subsidence ("basement" is defined herein as Pleistocene and underlying strata) versus processes in the shallow (Holocene) subsurface. A better quantification of these relative contributions is required to inform decisions regarding the mitigation of future wetland loss. If the majority of land surface lowering is due to shallow processes, restoration plans such as those set out in the Master Plan for coastal Louisiana [*Coastal Protection and Restoration Authority of Louisiana*, 2012] could anchor coastal-defense infrastructure in the basement and expect relative vertical stability over the design lifetime. If, on the other hand, basement subsidence is the main culprit, this task would be much more challenging. It is therefore of great importance to understand the processes that have contributed to the basement deformation history, as well as their relative importance and uncertainties.

Due to basinward steepening of Pleistocene river terraces in south Louisiana, it has long been presumed that subsidence in the MD contains a component of crustal movement and mantle flow caused by sediment loading, referred to herein as sedimentary isostatic adjustment (SIA). *Fisk* [1939] and a number of subsequent studies (notably *Fisk and McFarlan* [1955]) interpreted the observed land subsidence as being dominated by this process. The pattern of crustal motions identified by *Fisk* [1939] was subsequently confirmed by

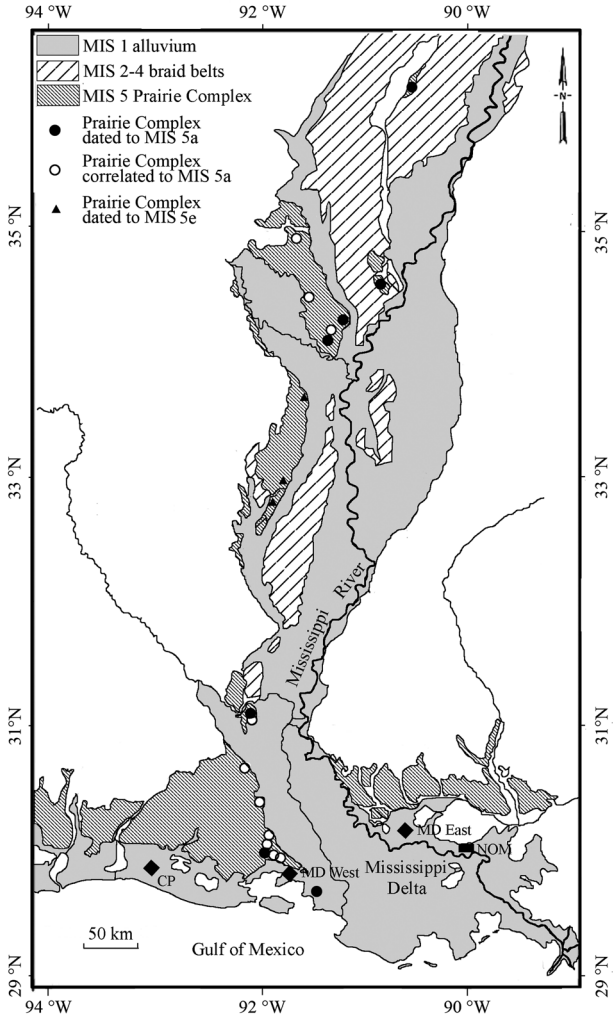

Figure 1. Generalized map of the late Quaternary geology of the Lower Mississippi Valley and Mississippi Delta (MD) (modified from *Saucier* [1994] and *Rittenour et al.* [2007]). The circles and triangles are core sites from *Shen et al.* [2012]. The diamonds show the Louisiana Chenier Plain (CP) locality of *Yu et al.* [2012], and the MD East and MD West localities refer to studies by *Törnqvist et al.* [2004, 2006] and *González and Törnqvist* [2009]. NOM = New Orleans metropolitan area.

benchmark leveling [*Burnett and Schumm*, 1983; *Jurkowski et al.*, 1984]. Modern subsidence rates of a few millimeters per year were obtained near the New Orleans metropolitan area (NOM) [*Jurkowski et al.*, 1984]. These values are generally consistent with global positioning system (GPS) measurements [*Dokka et al.*, 2006] and more recent leveling data analysis [*Dokka*, 2011].

Studies over longer (geologic) timescales concluded that SIA-induced subsidence rates are an order of magnitude lower than the geodetically inferred rates. RSL records for the past 8 kyr from compaction-free basal peat immediately overlying the Pleistocene basement in the MD provide rates largely similar to RSL records from tectonically stable areas away from the U.S. Gulf Coast [*Törnqvist et al.*, 2006]. Furthermore, as very little difference between RSL records from various portions of the MD was found, it appears that long-term subsidence rates of the basement are on the order of a fraction of 1 mm yr^{-1} [*Törnqvist et al.*, 2006]. *Yu et al.* [2012] compared the Holocene RSL data from the MD with a new RSL record from the Louisiana Chenier Plain (Figure 1) where SIA was predicted to be minimal [*Blum et al.*, 2008] and inferred a SIA-driven differential subsidence rate in key portions of the MD of only 0.15 ± 0.07 mm yr^{-1}. These contrasting subsidence rates were inferred from records that span significantly different timescales, which may suggest that measured rates depend on the time window of observation [e.g., *Meckel*, 2008; *Dokka*, 2011]. One way to address this problem is to quantify the contribution of basement subsidence due to SIA through geophysical modeling.

Previous modeling studies have produced a wide range of present-day subsidence rates. *Jurkowski et al.* [1984] predicted SIA subsidence rates of ~2 mm yr^{-1} near the NOM using a model that assumed a lithospheric thickness <40 km (as inferred here from their flexural rigidity value) and an upper mantle viscosity of 3×10^{19} Pa s. *Ivins et al.* [2007] calculated SIA subsidence rates of ~5 mm yr^{-1} near the NOM and up to 8 mm yr^{-1} near the southeast Louisiana shoreline using a model with a 50 km thick lithosphere and an upper mantle viscosity of 3×10^{20} Pa s. *Blum et al.* [2008] modeled SIA with a 30 km lithosphere and obtained late Holocene SIA subsidence rates up to ~1 mm yr^{-1} in the MD. *Syvitski* [2008] produced rates of ~2 to 6 mm yr^{-1} but provided few details on the relevant model parameters.

Due to the popular assumption that present-day land surface subsidence rates are dominated by SIA, these modeling studies were compelled to adopt relatively extreme values for either Earth model parameters [*Jurkowski et al.*, 1984] or load magnitudes [*Ivins et al.*, 2007] to match geodetically observed subsidence rates. However, the assumption that SIA is the dominant process is not necessarily correct. The MD is sufficiently

close to the previously glaciated regions of North America to be influenced by ongoing glacial isostatic adjustment (GIA) [e.g., *Potter and Lambeck*, 2003; *Milne and Mitrovica*, 2008]. Furthermore, the Holocene sediments of the MD, upon which observations of land lowering are often collected, are subject to ongoing compaction [*Törnqvist et al.*, 2008]. Finally, there is potential for fluid extraction or faulting to contribute to land surface lowering [*Morton and Bernier*, 2010; *Kolker et al.*, 2011; *Dokka*, 2011; *Yu et al.*, 2012]. Thus, it is perhaps not surprising that results between modeling studies have been inconsistent.

The present study takes a different approach. The focus is not on precisely tuning models to fit specific data but rather to establish whether the magnitude of both long-term vertical displacement and present-day deformation rates can be reasonably approximated when applying realistic loading histories and a broad but plausible range of Earth model parameters. Land subsidence caused by GIA (ice and ocean loading) as well as all major sediment bodies deposited in the region since the last interglacial is explicitly modeled. The Holocene delta loading history applied in this study is the most sophisticated to date. Eight different Earth models were used to span a wide but plausible range of parameter values. The results of this modeling allow a rigorous comparison with quantitative, geologic data for various timescales within the late Quaternary, in addition to present-day GPS records. Geologic data are essential, because geodetic data always concern timescales that are very short relative to the characteristic timescales of the processes of interest. The wide scope of this study and differing timescales of the data also allow the time-dependent aspects of deformation in this region to be examined. It is important to note that this study does not aim to make exact predictions of subsidence rates and their spatial variability; the modeling results should not be used in this way by future studies.

2. Observations

Three distinct types of data were used in this study. Present-day GPS records and Holocene RSL curves reconstructed from basal peat were used as a measure of relatively recent deformation rates. Longer-term total displacement (since ~80 ka) was determined from sampling the present-day height of the Marine Isotope Stage (MIS) 5a long profile of the Lower Mississippi River and comparing it with the shape of the nondeformed, modern long profile.

2.1. Present-Day Deformation Rates

Present-day rates of deformation in the MD region can be obtained by GPS measurements. GPS data are available since the mid-1990s and in principle can provide a good indicator of ground motion. *Dokka et al.* [2006] reported present-day deformation rates in and near the MD based on GPS measurements at 20 stations (Figure 2) over a 2–11 year time window. Data were collected using a combination of continuous recording and campaign measurements. An average subsidence rate of 5.2 ± 0.9 mm yr^{-1} for the MD was reported. The errors on the vertical GPS rates are relatively large and for many stations the error is of similar magnitude as the signal. It is important to note that the monuments of all GPS stations south of ~30°N are underlain by >10 m of Holocene sediment (Figure 2, blue numbers) and could therefore be subject to ongoing compaction.

2.2. Late Holocene Deformation Rates

It is also possible to obtain rates of vertical ground motion, averaged over the last few millennia, from Holocene RSL records. *Yu et al.* [2012] compared RSL curves from basal peat within the MD to a new RSL record outside the immediate delta load region (Figure 1, MD versus Chenier Plain (CP) localities). The data demonstrate a clear divergence in postglacial RSL rise between the MD and the CP where the latter plot ~1 m higher at 7 ka. Assuming that the differential subsidence is due to SIA and that the contribution of this process is zero at the CP locality, *Yu et al.* [2012] inferred a SIA-driven subsidence rate of 0.15 ± 0.07 mm yr^{-1} at the MD localities. This approach is useful as it provides an indication of geologically recent subsidence rates and effectively filters out the effects of GIA, which is a potentially significant contributor on a regional scale [e.g., *Potter and Lambeck*, 2003].

2.3. Late Quaternary Displacement and Rates

Few previous studies have used deformed long profiles in the alluvial reach of a continental-scale river to investigate the geodynamic effects of deltaic sediment loading. Numerous investigations [e.g., *Schumm et al.*, 2002, and references therein] have dealt with the effect of active tectonics on river evolution; however,

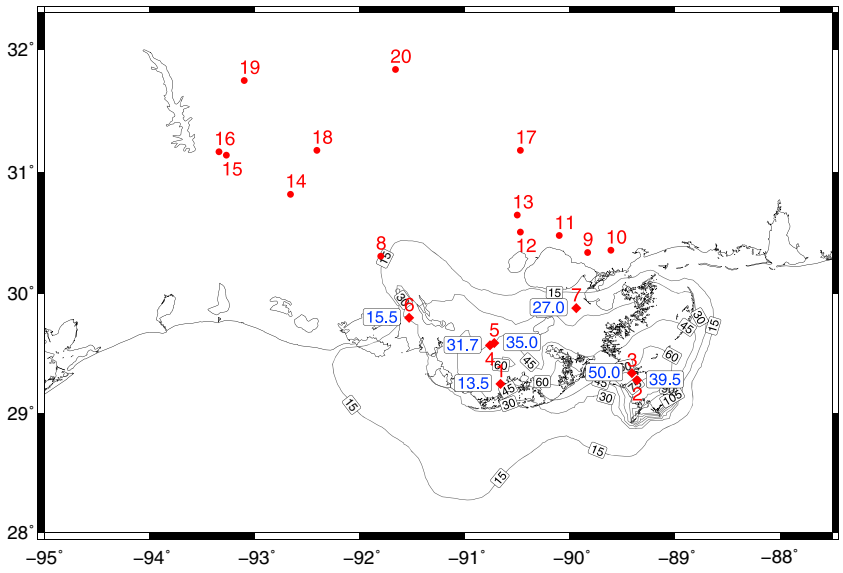

Figure 2. Location of GPS sites [*Dokka et al.*, 2006] in and near the Mississippi Delta; red numbers match those on the *x* axis of Figure 6. The isopach of the Holocene delta is from *Kulp et al.* [2002]. For GPS sites within the Holocene delta, the thickness of Holocene strata below the GPS monument (in m) is shown in blue, derived by subtracting the depth of the monument as reported by *Dokka et al.* [2006] from the total thickness of Holocene strata in the isopach map.

the methodology used in this study is significantly different. The Prairie Complex, a late Pleistocene allostratigraphic unit, is widely preserved along the western margin of the Lower Mississippi Valley (Figure 1) and was formed by a meandering precursor of the Lower Mississippi River and its tributaries [*Fisk*, 1944; *Saucier*, 1994]. *Shen et al.* [2012] showed that widespread portions of the Prairie Complex date to MIS 5a (~80 ka) and to a lesser extent MIS 5e (~120–130 ka). The spatial distribution of the MIS 5a Prairie Complex enables the height of the 80 ka Lower Mississippi River long profile relative to the present-day long profile to be obtained (Figure 3a).

Long profiles of large alluvial rivers are generally concave in shape on a regional scale [*Mackin*, 1948]; the present-day Lower Mississippi River natural-levee long profile conforms to this observation (Figure 3a). In contrast, the MIS 5a long profile is predominantly convex, suggesting that it has been distorted due to vertical land motion after floodplain abandonment and terracing following the MIS 5a/4 sea-level fall [*Shen et al.*, 2012]. The intersection of the MIS 5a and the present-day long profiles at 30.5°N is supported by abundant data, while an observational gap exists between about 31.5 and 34°N. However, uplift in that region is supported by the presence of a MIS 5e floodplain surface at an even higher elevation (Figure 3a).

The MIS 5a RSL highstand lasted for >5 kyr [e.g., *Dorale et al.*, 2010], while the present-day RSL highstand in the Gulf of Mexico was initiated ~7 ka [*Törnqvist et al.*, 2004]. Thus, at both times the long profile had >5 kyr to adjust after a major sea-level rise. The MIS 5a meander belts had a geometry and sediment texture similar to present-day conditions [*Fisk*, 1944; *Autin and Aslan*, 2001; *Rittenour et al.*, 2007; *Shen et al.*, 2012]. Furthermore, the surface elevation of the MIS 5a Prairie Complex at 35 to 36°N is similar to that of the present-day floodplain (Figure 3a), suggesting that MIS 5a relief was comparable to that of the modern Lower Mississippi River. With such similar boundary conditions, the two long profiles are likely to exhibit similar original shapes [e.g., *Snow and Slingerland*, 1987] but potentially different elevations due to RSL differences.

There are no published RSL records from the U.S. Gulf Coast precisely dated to MIS 5a. On the U.S. Atlantic Coast, RSL during this time increases northward from around −10 m (relative to present sea level) in southern Florida [e.g., *Ludwig et al.*, 1996] to a maximum of +10 m in Virginia [e.g., *Wehmiller et al.*, 2004]. *Potter and Lambeck* [2003] demonstrated that RSL in the wider region was likely to be somewhat higher than the global average due to intermediate-field GIA effects, where RSL has a reasonably strong dependence on the distance from the center of glaciation. In this context, given that the MD is located between southern Florida and Virginia, it is likely that MIS 5a RSL was within ±10 m of present sea level. The upstream distance over

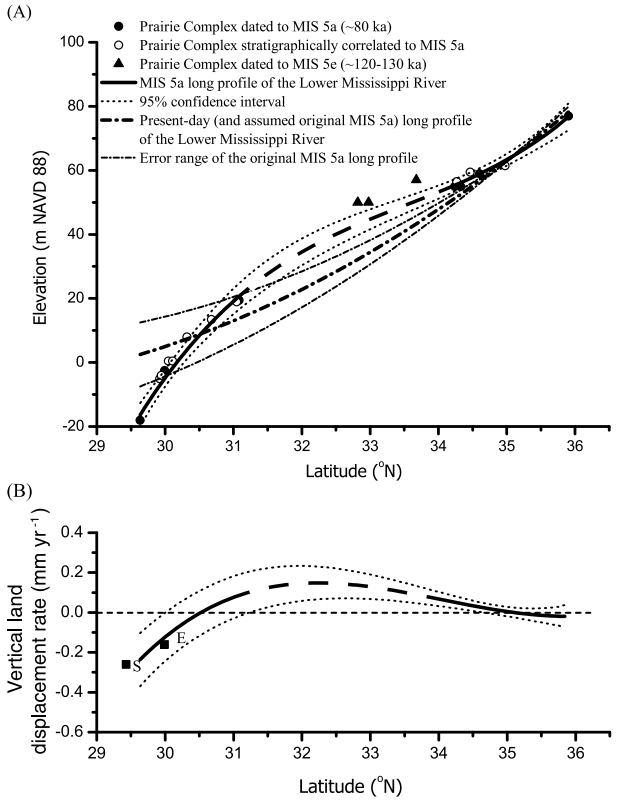

Figure 3. (a) Present-day and MIS 5a natural levee long profiles of the Lower Mississippi River. The Lower Mississippi Valley is approximately N-S oriented; thus, elevation is plotted against latitude. The present-day long profile is a second-order polynomial function fitted to 70 present-day natural levee elevation points, which corresponds to the long profile during bankfull discharge. Most of the MIS 5a Prairie Complex cores were taken on natural levees of the MIS 5a Mississippi River. The elevation of the MIS 5a terrace segments was obtained by subtracting the thickness of overlying loess and post-MIS 5a fluvial deposits (Table S1) [*Autin and Aslan*, 2001; *Shen et al.*, 2012] from the land-surface elevation. The MIS 5a long profile approximation is obtained by fitting a third-order polynomial function to the data points with optically stimulated luminescence age control (filled circles). No MIS 5a deposits were identified along the dashed part of the profile; this segment is unconstrained. However, the elevation of a MIS 5e terrace (filled triangles) supports the inferred uplift of this segment. (b) Rate of vertical land displacement in the Lower Mississippi Valley and the Mississippi Delta averaged over the past 80 kyr. Negative values represent subsidence, and positive values represent uplift. The filled squares are long-term subsidence rates reported by *Edrington et al.* [2008] (E) and *Straub et al.* [2009] (S).

which this uncertainty is likely to decay to zero can be derived from the landward extent of base-level control of the long profile of the Lower Mississippi River, estimated at ~600 km [*Rittenour et al.*, 2007; *Shen et al.*, 2012]. *Nittrouer et al.* [2012] demonstrated that channel morphology in the lowest ~600 km of the Lower Mississippi River is subject to a backwater effect. Due to the similar RSL during MIS 5a and at present, it is not expected that the backwater effect significantly influences the long profile comparison in this study.

Based on the reasoning outlined above, it was assumed that the present shape of the long profile is a good proxy of the original MIS 5a profile when assigned a vertical error of ±10 m at the shoreline, which linearly decreases to zero at a point 600 km north of the present coast. The net vertical displacement of the MIS 5a long profile was obtained by subtracting this reconstructed original MIS 5a profile from the observed MIS 5a long profile. Dividing this displacement by 80 kyr produces an estimate of the average deformation rates for this period based on the assumption that the land motion was monotonic at each location (Figure 3b). Rates follow the same spatial pattern as the total displacement, decreasing northward from 0.24 ± 0.13 mm yr^{-1} subsidence at 29.6°N to a hinge line with zero subsidence at 30.5°N. Farther north, uplift rates up to 0.15 ± 0.08 mm yr^{-1} are found. Displacement data at the MIS 5a core sites were obtained (Figure 3 and Table S1) for comparison with model output.

3. Modeling Approach

Present-day rates of deformation and the vertical motion of the 80 ka long profile were modeled using a Maxwell (viscoelastic) spherically symmetric Earth model [after *Peltier*, 1974] onto which sediment, ice, and ocean loads were applied. Output comprised vertical displacement of the MIS 5a long profile as well as present-day and Holocene deformation rates. This type of model is more commonly applied to investigate the effects of mass exchanges between land-based ice and the ocean at regional scales. The model is based on a spherical harmonic formalism, with the resolution defined by the specified truncation. A truncation of order 256, which results in a resolution of ~70 km, was used in most previous work with this specific model code [e.g., *Milne et al.*, 2001; *Bradley et al.*, 2009; *Milne and Peros*, 2013]. For this study, the truncation was extended to order 512, resulting in a ~35 km resolution. This allows the spatial evolution of the sediment loads (e.g., subdeltas) to be resolved and the ~100 km length scale of observed deformation to be captured.

Table 1. Structure of Earth Models as Defined by Three Parameters: Lithospheric Thickness (LT), Upper Mantle Viscosity (UMV), and Lower Mantle Viscosity (LMV)

LT (km)	UMV (Pa s)	LMV (Pa s)	Abbreviation
46	3.00E + 20	1.00E + 22	46/0.3/10
46	1.00E + 21	1.00E + 22	46/1/10
71	3.00E + 20	1.00E + 21	71/0.3/1
71	3.00E + 20	1.00E + 22	71/0.3/10
71	3.00E + 20	5.00E + 22	71/0.3/50
71	1.00E + 21	1.00E + 22	71/1/10
96	3.00E + 20	1.00E + 22	96/0.3/10
96	1.00E + 21	1.00E + 22	96/1/10

Significant uncertainty in the modeling of SIA and GIA relates to the viscosity structure of the adopted Earth model. In this study, Earth structure was defined by three parameters: the thickness (in km) of a high-viscosity (1×10^{43} Pa s) uppermost layer to simulate the lithosphere (referred to as lithospheric thickness, LT); the viscosity beneath this layer and extending to 660 km depth (referred to as upper mantle viscosity, UMV); and the viscosity from 660 km to the core-mantle boundary (referred to as lower mantle viscosity, LMV). These values are expressed as the triplet LT/UMV/LMV, with the second and third terms defined as multiples of 10^{21} Pa s. The radial elastic and density structures were taken from the Preliminary Reference Earth Model (PREM) [*Dziewonski and Anderson*, 1981], a significantly more realistic structure than that used by previous studies [e.g., *Ivins et al.*, 2007]. No significant differences between PREM and other available velocity/density models have been found for deformations with colatitudes $>1°$ [*Wang et al.*, 2012], validating the use of PREM in this study. The model was run with eight different Earth viscosity structures (Table 1). The selection of Earth parameters covers the range found by studies across different methodologies [e.g., *Peltier*, 1996; *Karato*, 2008]. Two layers of different viscosity within the mantle are considered sufficient when the depth sensitivity of the observations and the uncertainty in the actual viscosity structure are taken into account [*Mitrovica*, 1996; *Paulson et al.*, 2007].

GIA was modeled with the ICE-5G global ice model [*Peltier*, 2004] and an ocean load derived from ICE-5G using the sea-level theory and algorithm described in *Mitrovica and Milne* [2003] and *Kendall et al.* [2005], respectively. ICE-5G has been tested against a global distribution of both geologic and geodetic observations. Although no model can be perfectly accurate, it is considered to be one of the leading ice histories available and is widely employed. One example is the study by *Milne and Peros* [2013] which demonstrated that ICE-5G can provide high-quality fits to RSL data from the circum-Caribbean region (including data from the MD). The effects of GIA-induced changes in Earth rotation were incorporated [*Milne and Mitrovica*, 1998; *Mitrovica et al.*, 2005], even though the contribution is relatively small and does not alter the first-order sense of the deformation/displacement output. In addition to the more direct ice load-driven deformation, changing sea level (the ocean load) has a levering effect on continental margins, driven by predominantly global ocean volume-related depth changes on the continental shelf [*Clark et al.*, 1978; *Mitrovica and Milne*, 2002].

Sediment load histories for the past 80 kyr were extracted from published data; some were adopted directly, while others (specifically portions of the Holocene delta load) were newly constructed. Given the complex history of the Lower Mississippi River depocenter over the past glacial-interglacial cycle, the sediment load history is broken down into five components (Figure 4). This includes the spatial extent and total thickness of (1) the Holocene MD (henceforth referred to as "delta") from *Kulp et al.* [2002] which is further broken down into Mississippi River subdeltas (equivalent to what others have referred to as deltas, delta lobes, or delta complexes) based on data from *Fisk* [1944]; *Kolb and Van Lopik* [1966], and *Frazier* [1967]; (2) the submarine fan of the Mississippi system on the Gulf of Mexico seafloor ("fan") [*Stelting et al.*, 1986]; (3) the paleovalley of the Lower Mississippi River beneath the MD ("paleovalley") [*Blum et al.*, 2008]; (4) continental shelf sedimentation ("shelf") [*Coleman and Roberts*, 1988]; and (5) the Mississippi Canyon on the continental slope ("canyon") [*Coleman and Roberts*, 1988]. Some components (paleovalley and canyon) involve a phase of sediment removal (i.e., unloading); details are provided in Table 2.

The delta load was constructed by converting published sediment thicknesses from regionally correlated cores and seismic data into a gridfile format [*Kulp et al.*, 2002]. The fan, shelf, and canyon loads were constructed by tracing isopach data from georeferenced images of published maps using ArcMap. The paleovalley load was adopted from *Blum et al.* [2008] and is the crudest of the sedimentary load models considered here. Sediment loading was applied linearly over the time span of deposition (Table 2).

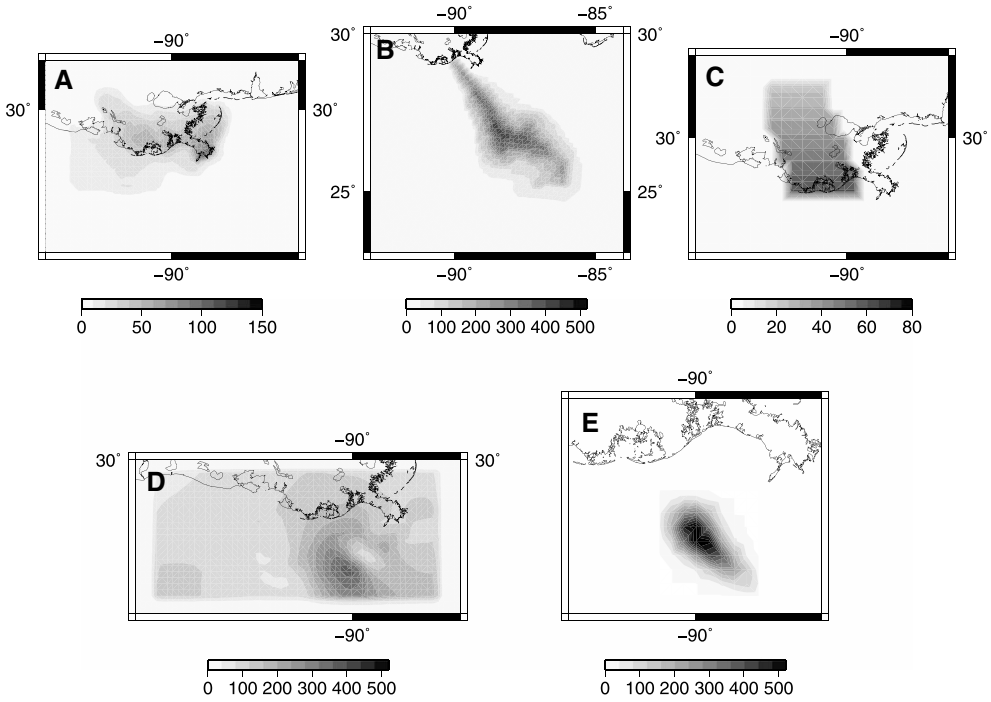

Figure 4. Sediment load models used in this study. (a) Delta, (b) fan, (c) paleovalley (load eroded and then redeposited), (d) shelf, and (e) canyon (load eroded and then redeposited). Load chronologies are provided in Table 2.

The timing of the end of deposition of the Mississippi Fan is uncertain [*Simms et al.*, 2007]. To assess the significance of this uncertainty, two scenarios were tested: one where submarine fan deposition ceased at 20 ka and a second where deposition continued until 10 ka.

Assigning sediment density is nontrivial and involves considerable uncertainty. Medium sand has a density of ~2000 kg m^{-3} [e.g., *Manger*, 1963]; clay and silt are less dense; a certain (albeit not well constrained) amount of low density organic matter is also present, notably in the delta. Bulk density data from the Holocene MD [*Kuecher et al.*, 1993] show values that cluster around 1500 kg m^{-3}. In marine settings, sediment deposited will displace its own volume of water. Thus, only the difference in density between water and sediment should be used. The additional loading that the displaced water applies through increasing the height of the water column is negligible. While the Holocene delta is thought to have predominantly prograded into marine waters, some portions have accumulated subaerially. Depending on the proportion of terrestrial (subaerial) deposition, the true effective density could therefore be higher than 500 kg m^{-3}. The linear response of the Earth model allows the impact of varying density to be easily evaluated. For a given Earth model, if the sediment density is doubled, the deformation rate and total magnitude is also doubled. This potentially large uncertainty (factor of 2) only applies to the delta load component; the relative importance of this uncertainty is described in section 4. Sediment densities for each load in this study are shown in Table 2.

Table 2. Time Intervals Over Which Load Models Were Applied With Sediment Density for Each Load[a]

Load	Time Interval (ka)	Density (kg m^{-3})
Delta	6–0	500
Canyon	29–22, 22–12	800
Paleovalley	30–11.5, 11.5–6	1500
Shelf	80–24	800
Fan	55–10	500
Ice	122–0	920
Ocean	122–0	1000

[a]For the canyon and the paleovalley loads, the first time interval is erosion and the second deposition.

There are potential uncertainties in the spatial distribution of the delta load over time. The total delta load (Figure 4a) was applied as a single load from 6 ka to present. In reality, the delta accumulated as a series of periodically switching subdeltas. To investigate the impact of

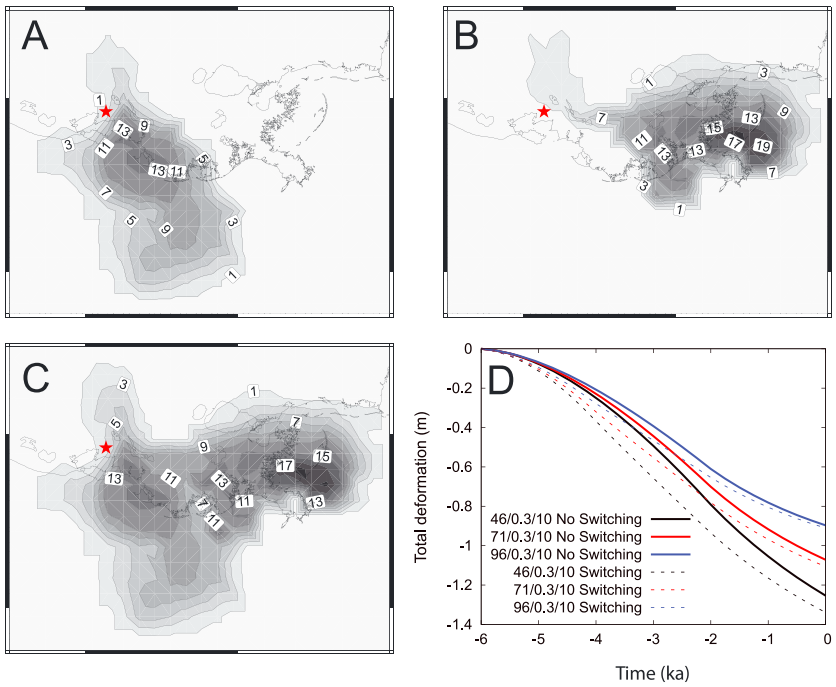

Figure 5. Subdelta switching sensitivity test. (a) Teche subdelta, load applied 6 to 4 ka; (b) St. Bernard subdelta, load applied 4 to 2 ka; and (c) combined Teche and St. Bernard subdeltas, load applied 6 to 2 ka as the nonswitching reference. Sediment thicknesses in meters, load density for the example shown here is 1500 kg m^{-3}. (d) Comparison of total deformation caused by the delta load at the MD West locality indicated by the red star in Figures 5a–5c. This site is located on the Teche subdelta and represents a location where the difference in spatial deformation pattern caused by the subdelta switching event is greatest.

subdelta switching, two trial loads were constructed. The first applied the Teche subdelta load between 6 and 4 ka, then switched to the St. Bernard subdelta between 4 and 2 ka, followed by no further loading between 2 ka and the present (note that the ages used in this sensitivity experiment do not necessarily reflect the true ages of the subdeltas involved). The second applied the sum of the two subdelta loads linearly from 6 ka to 2 ka with no further loading from 2 ka to present. The location and extent of the loads is shown in Figures 5a–5c. Three Earth models were used in this sensitivity test: 46 km, 71 km, and 96 km LT; all with 0.3/10 mantle viscosity (Table 1). The low value of UMV was chosen to produce maximum rates of deformation and thus a large response over the past 6 kyr. Deliberately high load densities of 1000 kg m^{-3}, 1500 kg m^{-3}, and 2000 kg m^{-3} were used to produce a plausible maximum effect.

4. Results

In this study there are two types of model run. A small number of targeted model runs were used to assess the significance of the load history uncertainties described above. The results of these initial runs are presented in section 4.1. Taking their outcomes into account, the full suite of Earth and load model combinations was then run. The results of the full suite are presented in sections 4.2 and 4.3.

4.1. Sensitivity to Load Models

The variability in deformation between runs with and without subdelta switching for the MD West locality is presented in Figure 5d. This locality is on the Teche subdelta, the area most sensitive to the modeled depocenter shift. Differences in displacement peak between 4 and 2 ka at ~10% (difference in height of the curves) for the most sensitive Earth model (46/0.3/10). When present-day subsidence rates are considered, the maximum differences at MD West between the load models with and without subdelta switching are 0.005–0.053 mm yr^{-1}, depending on the sediment density and Earth model. These differences are within the error reported for subsidence rates inferred from both GPS [*Dokka et al.*, 2006] and RSL [*Yu et al.*, 2012] data.

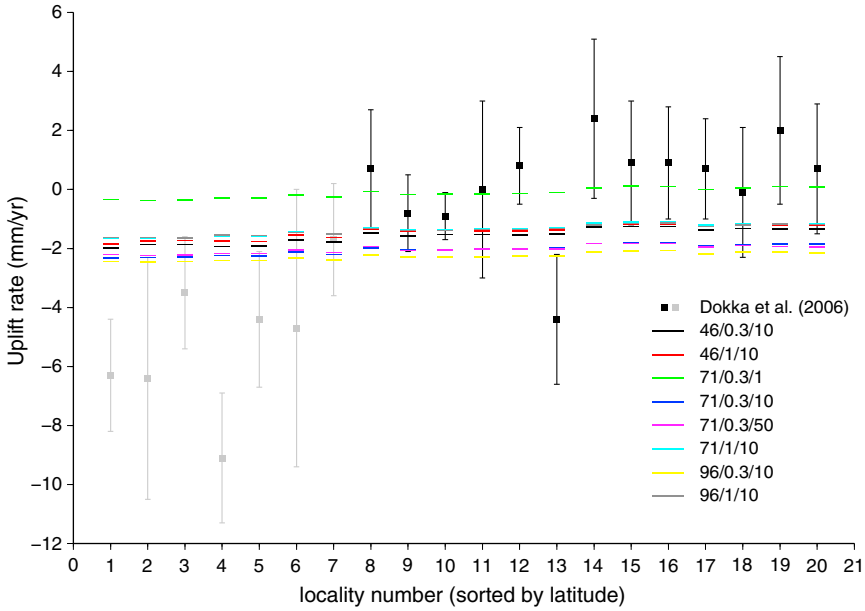

Figure 6. Comparison of deformation rates observed by *Dokka et al.* [2006] and modeled rates obtained with eight different Earth models (Table 1). Negative values indicate subsidence. Points in gray represent GPS monuments which are anchored within Holocene strata (see Figure 2). At such sites, the measured subsidence signal is likely to contain a sediment compaction signal of unknown magnitude. Error bars represent one standard deviation. Since there is longitudinal variation in the modeled rates (see Figure 7e), rather than comparing the observed and modeled rates as a function of latitude [e.g. *Dokka et al.*, 2006], they are compared site by site (site number increasing with latitude).

Differences in vertical displacement at present due to subdelta switching are extremely unlikely to exceed 0.283 m, a value produced with an excessively high sediment density.

When comparing the 10 ka to 20 ka end date for fan loading, present-day rates of vertical motion differ by less than 0.003 mm yr^{-1} between the two scenarios. This difference is insignificant with respect to the goals of this study. A 10 ka end of deposition was used for the fan in the main suite of runs.

The precise modeled density of the delta load, after correction for subaqueous deposition, is only of high significance when comparing output to the *Yu et al.* [2012] differential subsidence value. As detailed further below, for all other comparisons, the delta load makes a minor contribution to modeled rates of surface deformation and the total displacement.

Modeled present-day subsidence rates produced by the canyon load were of order 0.01 mm yr^{-1}, and total present-day displacement relative to the initial condition was $<$0.01 m. Due to the small magnitude of these values relative to observational uncertainty, the canyon was not included in the subsequent analysis.

4.2. Present-Day Deformation Rates

Present-day deformation rates were calculated at appropriate localities to allow comparison with data from *Dokka et al.* [2006] and *Yu et al.* [2012]. Only the delta, paleovalley, ice, and ocean loads produce deformation rates greater than data error for present-day rates. GIA signals dominate the absolute rates. The fan and shelf loads have essentially reached isostatic equilibrium and thus make a negligible contribution to present-day rates.

A comparison of the model output with deformation rates from GPS stations [*Dokka et al.*, 2006] is shown in Figure 6. The modeled vertical rates of basement deformation show a N-S signal that is an order of magnitude smaller than the GPS rates that exhibit a ~5 mm yr^{-1} increase south of 30.5°N (Figure 6). Comparing only the sites that are unlikely to be influenced by Holocene sediment compaction (plotted in black in Figure 6; Holocene sediment thicknesses underlying monuments of GPS stations are shown in Figure 2), the modeled pattern of subsidence rates is in agreement, to first order, with the GPS data. The apparent 1 to 2 mm yr^{-1}

Table 3. Rates of Vertical Land Motion in the Mississippi Delta Including All Loads for all Earth Models Considered (see Table 1)[a]

Locality	46/1/10	46/0.3/10	71/0.3/1	71/0.3/10	71/0.3/50	71/1/10	96/1/10	96/0.3/10
				SIA				
MD East	−0.40	−0.59	−0.39	−0.39	−0.39	−0.33	−0.26	−0.29
MD West	−0.29	−0.44	−0.32	−0.33	−0.33	−0.26	−0.22	−0.25
Chenier Plain	−0.09	−0.10	−0.14	−0.14	−0.14	−0.10	−0.11	−0.14
				GIA				
MD East	−1.16	−1.14	0.18	−1.73	−1.69	−1.11	−1.17	−2.04
MD West	−1.19	−1.19	0.15	−1.76	−1.69	−1.15	−1.19	−2.03
Chenier Plain	−1.17	−1.18	0.13	−1.73	−1.69	−1.12	−1.16	−1.98
				Total				
MD East	−1.56	−1.72	−0.20	−2.12	−2.08	−1.44	−1.43	−2.32
MD West	−1.48	−1.63	−0.17	−2.09	−2.01	−1.41	−1.41	−2.28
Chenier Plain	−1.26	−1.28	−0.00	−1.87	−1.82	−1.22	−1.27	−2.12
MD East-Chenier Plain	−0.30	−0.44	−0.20	−0.25	−0.26	−0.22	−0.17	−0.20
MD West-Chenier Plain	−0.22	−0.34	−0.16	−0.21	−0.20	−0.19	−0.15	−0.16

[a]Negative values indicate subsidence. The Chenier Plain locality (29.88°N, 93.12°W) is from *Yu et al.* [2012]. The MD East locality (30.07°N, 90.69°W) is an average of the Gramercy, Lutcher, and Zapp's sites [*Törnqvist et al.*, 2004]; the MD West locality (29.85°N, 91.73°W) is an average of the Delahoussaye Canal, Patout Canal, Lydia, and Glencoe sites [*Törnqvist et al.*, 2006; *González and Törnqvist*, 2009]. Rates are in mm yr^{-1}.

uniform offset between the average of the modeled and observed rates (sites 8 and higher) could, at least in part, be a systematic offset due to differences in geodetic reference frame between data and model [*Altamimi et al.*, 2007; *Wu et al.*, 2011]. However, the potential reference frame offset cannot explain the poor fit south of 30.5°N.

When comparing output to the data of *Yu et al.* [2012], it is the differential subsidence rate between their localities which must be considered. Table 3 contains a model reproduction of this comparison including both the GIA and SIA signals. The model produces differential subsidence rates, relative to the CP locality, of 0.17 to 0.44 mm yr^{-1} for the MD East locality and 0.15 to 0.34 mm yr^{-1} for the MD West locality (see also Figure 7e). The largest differential rates are produced by Earth models with a thin LT (46 km). The 96/1/10 Earth model yields a "closest fit" to the differential subsidence value found by *Yu et al.* [2012]. The values quoted above were produced with a delta load density of 500 kg m^{-3}; using a delta density of 1000 kg m^{-3} results in a range of 0.27 to 0.70 mm yr^{-1} for MD East and 0.24 to 0.54 mm yr^{-1} for MD West. With either density, the MD East and MD West localities exhibit similar values, consistent with their similar RSL histories [*Törnqvist et al.*, 2006]. Results for a delta load density of 500 kg m^{-3} are used in the following discussion because they provide a better match with the observations of *Yu et al.* [2012]. The differential subsidence rates shown in this study are generally higher than those observed [*Yu et al.*, 2012] and must be considered maximum values. Further work will be needed to refine model predictions to better match observations such as Holocene RSL curves.

Total subsidence rates are shown in Figure 7e, with individual components shown in Figures 7a–7d (using the "closest fitting" 96/1/10 Earth model). As the majority of the modeled (absolute) subsidence is due to GIA rather than SIA, the ongoing peripheral bulge collapse due to the melting of the Laurentide Ice Sheet (Figure 7d) [cf. *Milne and Mitrovica*, 2008] is of particular importance. Figure 7c illustrates the continental levering signal associated with ocean loading, with the gradient running approximately perpendicular to the shoreline and a landward transition from subsidence to uplift [*Clark et al.*, 1978; *Mitrovica and Milne*, 2002]. Considered together, the ice and ocean load response does not contribute significantly to the spatial pattern of deformation. The ice and ocean load signals have opposite spatial trends, with the uplift due to ocean loading in the north canceling much of the N-S spatial variability of the ice load signal.

Considering the magnitude of absolute subsidence, all Earth models except 71/0.3/1 produce total present-day subsidence rates in the 1 to 2.5 mm yr^{-1} range in the MD; rates due to MD SIA alone range from 0.35

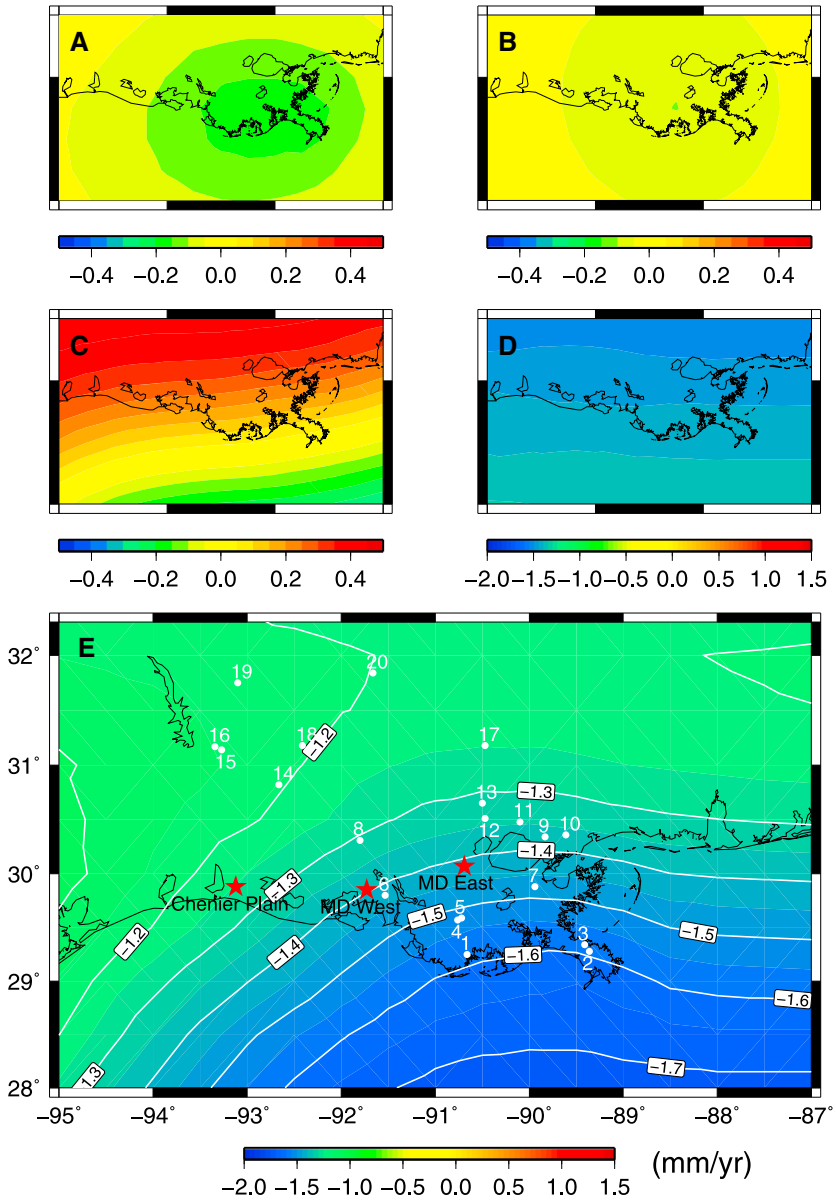

Figure 7. Present-day vertical deformation rates obtained with Earth model 96/1/10. This Earth model provides the closest fit to the differential RSL data of *Yu et al.* [2012] but does not represent a precisely tuned prediction of subsidence rates. (a) Delta load, (b) paleovalley load, (c) ocean load, (d) ice load, and (e) all loads. In Figure 7e, red stars are localities MD East [*Törnqvist et al.*, 2004], MD West [*Törnqvist et al.*, 2006; *González and Törnqvist*, 2009], and Chenier Plain [*Yu et al.*, 2012]. White dots are GPS sites from *Dokka et al.* [2006]; numbers match those in Figure 6. All color scales are in mm yr^{-1}, but note that Figures 7a–7c are plotted using a finer color scale than Figures 7d and 7e. The other model runs in this study display a similar pattern. Note that the geographic area considered in Figure 7e is slightly larger than that in Figures 7a–7d.

to 0.58 mm yr^{-1} (Table 3). Model 71/0.3/1 produces a much smaller total subsidence rate due to the very different GIA signal. With a low LMV, the peripheral bulge caused by the North American ice sheets has mostly subsided by the present day. Thus, the ocean load signal dominates the ice load signal, resulting in net isostatic uplift from the GIA component. The influence of the sediment load ensures that there is still subsidence in the region for the 71/0.3/1 Earth model and the differential subsidence rates between the MD and Chenier Plain are within the range of the other Earth models. This example clearly demonstrates the importance of the GIA signal as a component of absolute subsidence rates.

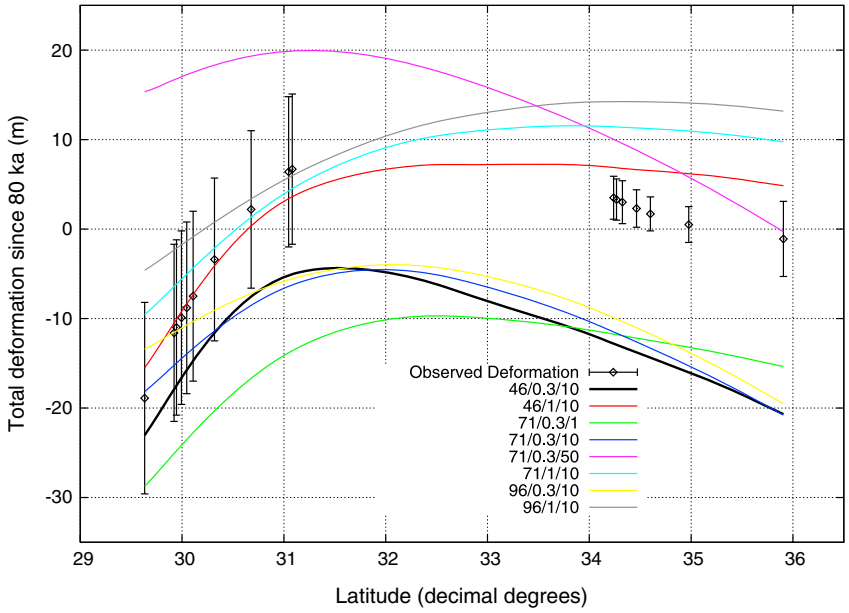

Figure 8. Total displacement since 80 ka (MIS 5a) for the eight Earth models considered (Table 1). Diamonds indicate MIS 5a long profile vertical displacement; error bars represent one standard deviation.

4.3. Long Profile Vertical Displacement

A comparison between the MIS 5a river long profile vertical displacement and the output from the model since 80 ka is shown in Figure 8; Figure 9 illustrates the contribution from individual loads. The modeled long profiles with an UMV of 1×10^{21} Pa s reproduce the overall shape of the observed

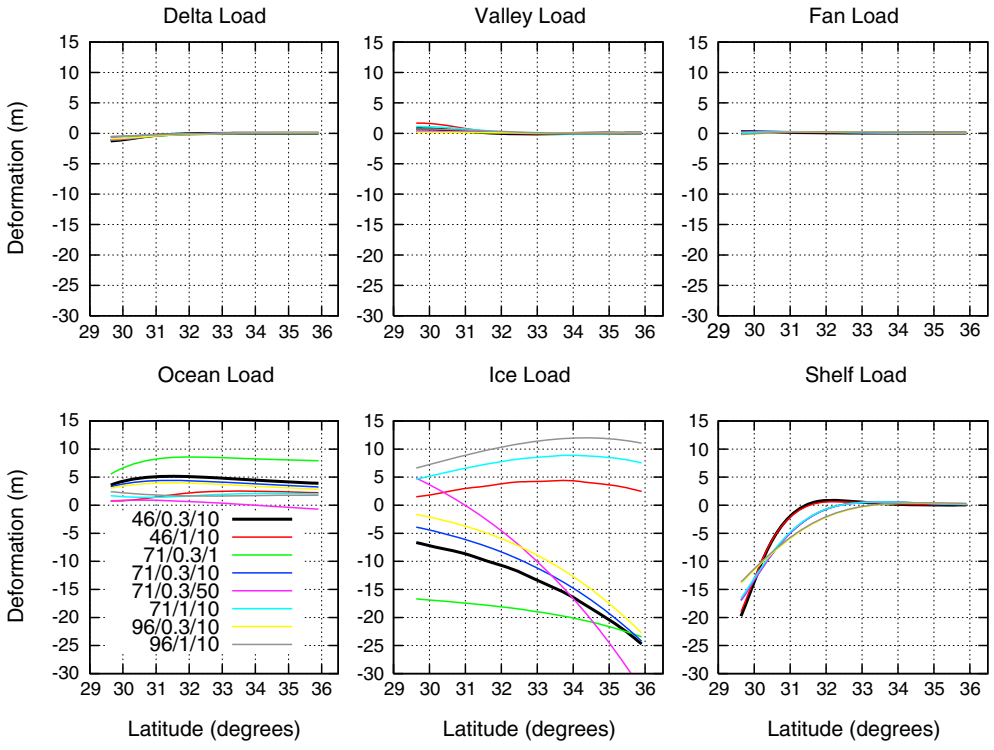

Figure 9. Individual components of total vertical displacement since 80 ka for each load and Earth model. These curves were summed to produce Figure 8.

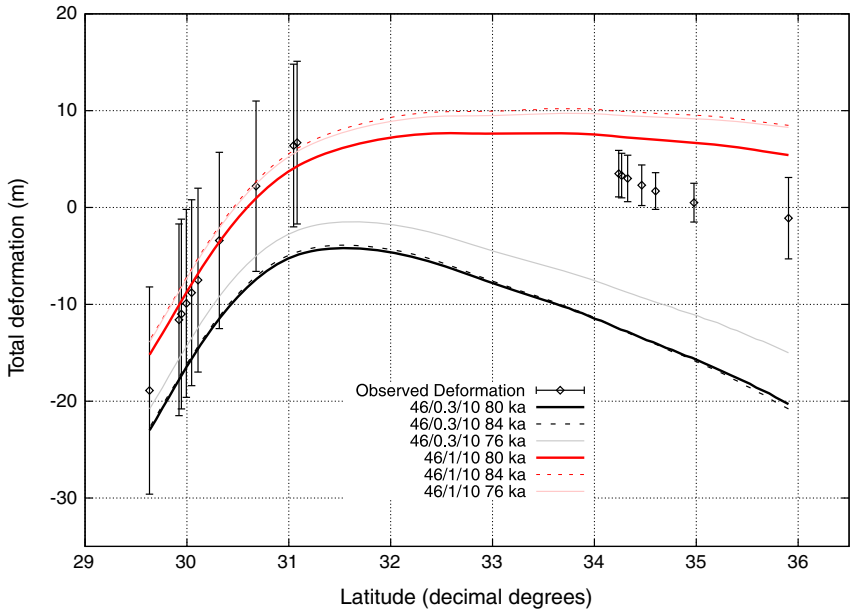

Figure 10. Estimates of the uncertainty in the ice load signal obtained due to uncertainties in the load chronology around 80 ka. Dashed lines indicate vertical displacement at present relative to the time indicated in the key. Times are 4 kyr before and after 80 ka. Note that in ICE-5G, 80 ka is a local minimum in North American ice volume; the sign of the effect of considering ice extent at earlier and later times is the same. The Earth models shown were chosen as they bracket the data reasonably well and represent some of the weakest Earth models used, producing the maximum variation in displacement.

displacement to first order. Models with an UMV of 3×10^{20} Pa s consistently underpredict the positive displacement north of 30.5°N. The closest fitting Earth model is 46/1/10, although better fitting Earth models are conceivable. In terms of the major contributors to long profile displacement (Figure 9), the 80–24 ka shelf load provides the steep downward displacement in the south, the ocean load provides the overall uplift, and the ice load provides the downward displacement in the north. The relatively low response to the ocean load when compared to the ice load is due to the difference in scale between the ~100 m change in global sea level and the ~1000 m change in land surface height in glaciated regions since 80 ka. In an intermediate field location like the MD, the ice signal dominates the ocean signal. The ice load in particular is very sensitive to the range of Earth model parameters considered. The two different UMV values produce the two separate groupings in the model output for this component of the signal. The delta, paleovalley, and fan loads together contribute only 1–3 m to the long profile displacement. The small contribution from the delta load renders uncertainties in its average density insignificant for this comparison. The paleovalley load provides a small upward displacement, reflecting the erosional portion of its history.

Earth models 71/0.3/1 and 71/0.3/50 produce a particularly poor fit to the vertical displacement data (Figure 8). However, the 71/0.3/50 Earth model fits the most northerly point, while the 71/0.3/1 Earth model fits the most southerly point, indicating that lateral variations in Earth structure could be important for the GIA component.

Due to the lack of well-constrained evidence for North American ice extent before the Last Glacial Maximum, there is uncertainty concerning the actual ice load at 80 ka [*St-Onge*, 1987; *Vincent and Prest*, 1987; *Kleman et al.*, 2010; *Stokes et al.*, 2012]. At 80 ka, there is a local minimum in the ICE-5G reconstruction of North American ice extent. To test the impact of this uncertainty, long profiles for the best-fitting 46 km LT Earth models were extracted for displacements relative to 84 ka and 76 ka (Figure 10). The results indicate a potential ~5 m perturbation of the long profile due to time uncertainty in the ice model with some sensitivity to UMV. The effect on the ocean load signal is a ~0.1 m perturbation, much less significant than uncertainties associated with the ice and shelf sediment loads.

5. Discussion

While the range of Earth and load models applied here is considerably wider than those of previous studies, it is important to be aware of model limitations and uncertainties. There is no erosion in the continental hinterland to act as a source for the sediment that is being deposited, so sediment mass is not conserved in the model. Similarly, there is no sediment reworking within the Lower Mississippi River system. Given the minimal importance of subdelta switching and the canyon load, these limitations are unlikely to affect the conclusions of this study. The physics implemented in the model does not permit faulting, an abundant phenomenon along the U.S. Gulf Coast [e.g., *Murray*, 1961]; the model does not explicitly consider salt tectonics. The potential impact of these two processes is therefore not addressed.

With respect to temporal uncertainty, all loads that were in place before ~10 ka contribute no measurable present-day deformation. Understanding the total displacement for these components is therefore only dependent on knowing the total sediment load.

5.1. Present-Day Deformation Rates

Present-day deformation rates appear to be dominated by ice, ocean, delta, and paleovalley loads. The model outputs do not support present-day basement subsidence rates greater than ~2 mm yr^{-1}. When considering SIA only, this is reduced to ~0.5 mm yr^{-1}. These values are in general agreement with stratigraphic studies [e.g., *Stanley et al.*, 1996; *Yu et al.*, 2012] but in conflict with previous modeling [*Jurkowski et al.*, 1984; *Ivins et al.*, 2007; *Syvitski*, 2008] (and to a lesser extent, *Blum et al.*, [2008]) which quote rates up to 8 mm yr^{-1} due to SIA only. Of these previous studies, that by *Ivins et al.* [2007] is the most comprehensive. The differences between their results and those presented here are due primarily to their delta load model; *Ivins et al.* [2007] significantly overestimated the delta volume. Dividing the sediment volumes of subdeltas used by *Ivins et al.* [2007] by the surface areas of these subdeltas reported by *Coleman et al.* [1998] yields average subdelta thicknesses of 50 m. It has long been known [e.g., *Kulp et al.*, 2002, 2005, and references therein] that across most of the MD the thickness of Holocene subdeltas is closer to ~15 m or less. Also, *Ivins et al.* [2007] adopted a high sediment density of 2050 kg m^{-3} and did not account for the reduction in effective density associated with marine deposition. These differences in the load model, in addition to their relatively low values for LT (50 km) and UMV (3×10^{20} Pa s), explain why the subsidence rates modeled by *Ivins et al.* [2007] exceed those inferred from RSL observations [e.g., *Yu et al.*, 2012] by an order of magnitude. *Blum et al.* [2008] modeled SIA subsidence rates closer to our results, but their rates should be considered maximum estimates because of the relatively thin LT (30 km) and low UMV (4×10^{20} Pa s) used.

Syvitski [2008] suggested that subdelta switching has a significant effect on SIA-induced deformation rates over the past 6 kyr. Unfortunately, the lack of information regarding the Earth model and sediment density used in that study precludes a direct comparison. It seems likely that the model of *Syvitski* [2008] implemented a very low mantle viscosity, based on a relatively short relaxation time of 2.5 kyr [*Hutton and Syvitski*, 2008]. Our sensitivity test indicates that the influence of subdelta switching can be considered negligible (within data uncertainty) for the purposes of the present study, consistent with Holocene RSL reconstructions from different portions of the MD [*Törnqvist et al.*, 2006].

Comparison with the GPS data [*Dokka et al.*, 2006] results in a poor overall fit. The uncertainty in the delta load density is not the cause of the poor fit because the delta load contribution is ~5 times smaller than the GIA contribution for most Earth models (Table 3). In addition, when the error margins in the GPS data are taken into consideration, a factor of 2 uncertainty in the delta load subsidence rate is of low significance. Given the wide range of Earth models considered, it is therefore likely that the GPS signal includes sources of subsidence other than SIA and GIA. This departure between modeled and observed rates may also support suggestions that there are recent accelerations in subsidence rate due to groundwater [*Dokka*, 2011] and/or hydrocarbon withdrawal [*Morton and Bernier*, 2010; *Kolker et al.*, 2011; *Chang et al.*, 2014]. While fluid withdrawal could impact certain localities, the primary candidate for the wider discrepancy is the compaction of Holocene strata. As an example, the 71/0.3/1 Earth model is able to fit sites judged unlikely to be influenced by Holocene sediment compaction (Figure 6, black data). This supports previous inferences [e.g., *Törnqvist et al.*, 2008; *Blum and Roberts*, 2012; *Simms et al.*, 2013] that GPS data from the MD and the adjacent U.S. Gulf Coast are likely to be influenced by sediment compaction. Specifically, *Törnqvist et al.* [2008] demonstrated that compaction remains significant in deeply buried Holocene deltaic strata.

This study finds that the *Yu et al.* [2012] data favor a relatively thick lithosphere (~96 km, possibly more). A subaerial paleovalley with erosion followed by deposition [cf. *Blum et al.*, 2008] and a low effective sediment density for the delta are also required, indicating predominant deposition in a marine setting. For all thinner LT values, differential subsidence rates are significantly overpredicted.

Yu et al. [2012] assumed that longitudinal variation in GIA effects was negligible between their chosen localities and that differences between RSL records were the product of SIA in the MD. The modeling presented here suggests that the GIA variation between the *Yu et al.* [2012] localities is less than 0.06 mm yr^{-1} (Table 3) and so within their data error. Thus, the majority of the observed differential subsidence is indeed likely to be produced by the delta and paleovalley loads. *Yu et al.* [2012] aimed to test the conclusions of *Blum et al.* [2008] and in doing so adopted the assumption that their Chenier Plain locality lies outside the bowl of subsidence caused by the MD load. Figures 7a and 7e indicate that this assumption is not entirely accurate; the differential deformation rate of 0.15 ± 0.07 mm yr^{-1} from *Yu et al.* [2012] is therefore likely to be a lower bound on ongoing SIA relative to a hypothetical stable locality outside the region.

González and Törnqvist [2009] used basal peat records to obtain a 0.6 ± 0.1 mm yr^{-1} (1σ error calculated from *González and Törnqvist* [2009, Figure 6a]) rate of RSL rise at the MD West locality between 1.4 and 0.4 ka. Using an average rate of RSL rise over such a short period as a proxy for deformation may be somewhat imprecise; the ocean surface is unlikely to be a stable reference during this period due to short-term climate fluctuations such as the Medieval Warm Period. However, ignoring this possible variation and assuming that ocean syphoning due to GIA was the dominant contributor to sea surface height change during this period, correcting for this effect (~0.3 mm yr^{-1}) [*Mitrovica and Milne*, 2002] results in a vertical land motion rate of ~1 mm yr^{-1} (note that we also assume zero eustatic sea-level change during this period). This value of total deformation (SIA plus GIA) is bracketed by the modeling results for the MD West locality (Table 3). Overall, the results are broadly consistent with the work of *Milne and Peros* [2013] who successfully modeled the Holocene RSL record of the MD using slightly higher LT values of 120 km.

5.2. Long-Term Vertical Displacement

Model results are capable of reproducing the magnitude and shape of Lower Mississippi River long profile vertical displacement over the past 80 kyr. Figure 8 indicates that an Earth model with a 46 km LT, an UMV between 3×10^{20} and 1×10^{21} Pa s, and a LMV of ~5×10^{21} Pa s would be capable of fitting the data. These values suggest a 5–16× UMV/LMV contrast, a range consistent with previous isostasy-based studies [*Mitrovica*, 1996; *Lambeck and Johnston*, 1998].

The present shape of the MIS 5a long profile is a composite of different load signals (Figure 9). This interpretation differs substantially from previous studies of deformation in and beyond the MD [e.g., *Fisk*, 1939; *Jurkowski et al.*, 1984], which attributed displacements to delta loading only. The largest consistent component of displacement (10–20 m, potentially higher seaward of the study area) is the continental shelf loading between about 80 and 24 ka. The ice load introduces the greatest amount of uncertainty as it is very sensitive to the Earth model (Figures 9 and 10). Net ocean loading between 80 ka and the present is relatively small (~10 m). However, as the LGM and subsequent deglaciation takes place in the last quarter of the time span considered, a continental levering effect (~5 m, Figure 9) was produced by the model. The ocean load signal counteracts to some extent that due to ice loading.

Given that the shelf load contributes such a large amount of vertical displacement to the MIS 5a long profile, uncertainties in the size of this load could have a significant impact. The shelf load model used (Figure 4d) is of somewhat limited lateral extent, particularly in the east, due to inherited spatial limits from the source [*Coleman and Roberts*, 1988]. It is therefore likely that the modeled shelf load values presented here are a lower bound on the amount of displacement produced by this load.

The timing of those loads not presently in equilibrium has some bearing on the predicted deflection of the MIS 5a long profile. The delta and paleovalley load histories are reasonably well constrained in time [*Kulp et al.*, 2002; *Blum et al.*, 2008] and contribute a relatively small amount (order meters) to the total modeled signal. The ice load results in ongoing subsidence of the peripheral bulge from the North American ice sheets. Major (deglacial) ocean load changes only ceased ~7 ka [*Törnqvist et al.*, 2004], and several meters of uplift can be expected from that component in the future. When considering all signals together, the ocean

loading-derived uplift is masked by the much larger subsidence rates from other components. The ocean load signal does, however, have an impact on the spatial pattern of the deformation signal (Figure 9).

For the best fitting Earth model (46/1/10), the contribution from GIA over 80 kyr is relatively small (<5 m) (Figure 9, red curve). This is due to the canceling of positive and negative displacements over a full glacial cycle [cf. *Potter and Lambeck*, 2003]. This approximate cancelation of the GIA signal suggests that calculating 80 kyr average deformation rates (Figure 3b) is a valid approach for estimating the order of magnitude of long-term subsidence rates due to SIA in the MD. These average rates are significantly smaller than the present-day deformation rates but are compatible with rates of ~0.16 mm yr^{-1} for the past ~15 Ma [*Edrington et al.*, 2008] and ~0.26 mm yr^{-1} for the past ~10 Ma [*Straub et al.*, 2009] (Figure 3b). Post-Miocene strata underneath the MD exhibit thicknesses that vary by no more than a factor of 2 along strike [*Woodbury et al.*, 1973], suggesting that strike variability of subsidence rates over this time frame is unlikely to be more than twofold.

In summary, long-term average basement subsidence rates in the MD since the Miocene have most likely been dominated by SIA, but instantaneous rates of subsidence are likely to be due to GIA processes. The modeling presented in this study suggests that present-day subsidence rates are higher than geologic averages.

5.3. Elastic Thickness of the Lithosphere

MIS 5a long profile vertical displacement data appear to favor Earth models with a LT of 46 km, whereas RSL-based subsidence rates over the past 7 kyr require Earth models with thicker LT (~96 km, possibly thicker). Thus, the optimal value for LT appears to be time dependent. This result is compatible with current understanding of lithospheric structure. The models implemented here adopt a simple "slab" lithosphere, which was assigned a single very high viscosity value throughout the specified thickness. While this is a common approach in most GIA studies, it is known that the lithosphere exhibits distinct rheological layering [*Afonso and Ranalli*, 2004; *Bürgmann and Dresen*, 2008]. Such layering would result in a thinning of the effective elastic thickness over time by flow and stress relaxation within the lithosphere [*Watts*, 2001]. More complex lithospheric models, based on a viscosity decrease linked to an assumed temperature profile, have been used in previous studies [e.g., *Klemann and Wolf*, 1998], although the exact mechanisms of lithospheric stress relaxation remain unclear [*Watts et al.*, 2013].

5.4. Future Work

The modeling presented here implemented a spherically symmetric Earth model. Tuning to RSL records and running a more finely incremented ensemble of models within the bounds of the solid Earth parameters defined by this study would allow specific best fit Earth models to be identified. However, seismic tomography studies [e.g., *Ritsema et al.*, 2011] indicate that there is significant lateral structure within the mantle, which could influence surface deformation. The lithosphere also varies laterally in thickness [e.g., *Tesauro et al.*, 2012]; this could impact model predictions. Codes that are able to implement Earth models incorporating 3-D viscosity structure exist [e.g., *Latychev et al.*, 2005; *Whitehouse et al.*, 2006]; implementing these models would be an important extension of the present study.

The ocean load model adopted here was calculated in a gravitationally self-consistent manner with respect to the adopted ice load model [*Mitrovica and Milne*, 2003; *Kendall et al.*, 2005]. However, the sediment load will also influence sea level through changes in sea floor height and perturbations to the gravity field. Application of a new extension to the sea-level equation [*Dalca et al.*, 2013], which computes a gravitationally self-consistent ocean load change with respect to both the ice and sediment redistribution histories, would be another route to extend the present analysis. While the improvements outlined above may help to resolve higher-order effects, the present study has demonstrated that with a relatively simple three-layer Earth, it is possible to understand the broad characteristics of the system and achieve reasonable fits to data.

6. Conclusions

It has been postulated that deltaic sediment loading is primarily responsible for the tilting of Pleistocene surfaces in the MD and Lower Mississippi Valley [*Fisk*, 1939]. This idea was extended to infer that the isostatic response to the delta load is the largest contributor to present-day subsidence in the region [e.g., *Jurkowski et al.*, 1984; *Ivins et al.*, 2007; *Syvitski*, 2008]. The primary aim of this study was to test this hypothesis by

means of a sensitivity analysis implementing a solid Earth deformation model and a full consideration of ice, ocean, and sediment loading histories. Comparing the model results with observations of vertical land motion obtained from different methods over a range of timescales (past 80 kyr, past 7 kyr, and past ~15 years) demonstrates that this hypothesis must be rejected. High rates of basement subsidence inferred from GPS sites within the MD are not reproducible when using realistic estimates of SIA and GIA.

Present-day Pleistocene basement subsidence in the MD produced by viscoelastic deformation mechanisms is unlikely to exceed ~2 mm yr^{-1}; subsidence due to sediment loading alone is unlikely to exceed ~0.5 mm yr^{-1}. The modeling results do not support basement subsidence rates of up to ~8 mm yr^{-1} proposed by previous modeling studies. It is likely that the large measured subsidence rates found in GPS, benchmark leveling, and tide-gauge data are the product of basement subsidence combined with significant ongoing Holocene sediment compaction. Contrary to some previous interpretations, it appears that SIA is unlikely to be the dominant cause of land surface lowering in the MD.

The ice load component of GIA is a major contributor to absolute vertical isostatic land motion along the U.S. Gulf Coast over timescales shorter than a full glacial cycle. Any future study which seeks to understand deformation along the U.S. Gulf Coast must consider both GIA and SIA. Which specific loads are most significant depends on the timescale considered.

The significance of the SIA components considered here also depends on the timescale considered. Over the past 80 kyr, the most important contribution to SIA in the MD region was likely to have been sedimentation on the continental shelf. In contrast, the Holocene delta is the most important source of present-day SIA-related basement subsidence.

Comparison of model results with geologic data over different timescales shows that the effective elastic thickness of the lithosphere is time dependent. The effective elastic thickness of the lithosphere may be $>$100 km over the Holocene but decreases by at least 50% to ~50 km on the 100 kyr timescale. The latter value is compatible with previous estimates of effective elastic lithospheric thickness for the region [e.g., *Bechtel et al.*, 1990], which considered loads applied over timescales considerably longer than those in this study.

Acknowledgments

Data supporting Figures 3a and 8 are available as in supporting information Table S1. All the other data for this paper are available on request. G.A.M. and M.W. acknowledge funding support from the Canada Research Chairs program and the University of Ottawa. T.E.T. acknowledges funding from the American Chemical Society—Petroleum Research Fund (award 39240-AC8). Z.S. was partly supported by the Long-term Estuary Assessment Group (LEAG) Program through the Tulane/Xavier Center for Bioenvironmental Research. M.W. would like to thank Ryan Love for modeling assistance.

References

Afonso, J. C., and G. Ranalli (2004), Crustal and mantle strengths in continental lithosphere: Is the jelly sandwich model obsolete?, *Tectonophysics*, *394*, 221–232, doi:10.1016/j.tecto.2004.08.006.

Altamimi, Z., X. Collilieux, J. Legrand, B. Garayt, and C. Boucher (2007), ITRF2005: A new release of the International Terrestrial Reference Frame based on time series of station positions and earth orientation parameters, *J. Geophys. Res.*, *112*, B09401, doi:10.1029/2007JB004949.

Autin, W. J., and A. Aslan (2001), Alluvial pedogenesis in Pleistocene and Holocene Mississippi River deposits: Effects of relative sea-level change, *Geol. Soc. Am. Bull.*, *113*(11), 1456–1466, doi:10.1130/0016-7606(2001)113.

Bechtel, T. D., D. W. Forsyth, V. L. Sharpton, and R. A. F. Grieve (1990), Variations in effective elastic thickness of the North American lithosphere, *Nature*, *343*, 636–638, doi:10.1038/343636a0.

Blum, M. D., and H. H. Roberts (2012), The Mississippi Delta region: Past, present, and future, *Annu. Rev. Earth Planet. Sci.*, *40*, 655–683, doi:10.1146/annurev-earth-042711-105248.

Blum, M. D., J. H. Tomkin, A. Purcell, and R. R. Lancaster (2008), Ups and downs of the Mississippi Delta, *Geology*, *36*(9), 675–678, doi:10.1130/g24728a.1.

Bradley, S. L., G. A. Milne, F. N. Teferle, R. M. Bingley, and E. J. Orliac (2009), Glacial isostatic adjustment of the British Isles: New constraints from GPS measurements of crustal motion, *Geophys. J. Int.*, *178*, 14–22.

Bürgmann, R., and G. Dresen (2008), Rheology of the lower crust and upper mantle: Evidence from rock mechanics, geodesy, and field observations, *Annu. Rev. Earth Planet. Sci.*, *36*, 531–567, doi:10.1146/annurev.earth.36.031207.124326.

Burnett, A. W., and S. A. Schumm (1983), Alluvial-river response to neotectonic deformation in Louisiana and Mississippi, *Science*, *222*, 49–50, doi:10.1126/science.222.4619.49.

Chang, C., E. Mallman, and M. Zoback (2014), Time-dependent subsidence associated with drainage-induced compaction in Gulf of Mexico shales bounding a severely depleted gas reservoir, *Am. Assoc. Petrol. Geol. Bull.*, *98*, doi:10.1306/11111313009, in press.

Clark, J. A., W. E. Farrell, and W. R. Peltier (1978), Global changes in postglacial sea level: A numerical calculation, *Quat. Res.*, *9*, 265–287, doi:10.1016/0033-5894(78)90033-9.

Coastal Protection and Restoration Authority of Louisiana (2012), Louisiana's Comprehensive master plan for a sustainable coast, Coastal Protection and Restoration Authority of Louisiana, Baton Rouge, 189 pp.

Coleman, J. M., and H. H. Roberts (1988), Sedimentary development of the Louisiana continental shelf related to sea level cycles: Part I—Sedimentary sequences, *Geo-Marine Lett.*, *8*, 63–108.

Coleman, J. M., H. H. Roberts, and G. W. Stone (1998), Mississippi River delta: An overview, *J. Coastal Res.*, *14*, 698–716.

Dalca, A. V., K. L. Ferrier, J. X. Mitrovica, J. T. Perron, G. A. Milne, and J. R. Creveling (2013), On postglacial sea level—III. Incorporating sediment redistribution, *Geophys. J. Int.*, *194*, 45–60, doi:10.1093/gji/ggt089.

Day, J. W., Jr., et al. (2007), Restoration of the Mississippi Delta: Lessons from Hurricanes Katrina and Rita, *Science*, *315*, 1679–1684, doi:10.1126/science.1137030.

Dokka, R. K. (2011), The role of deep processes in late 20th century subsidence of New Orleans and coastal areas of southern Louisiana and Mississippi, *J. Geophys. Res.*, *116*, B06403, doi:10.1029/2010jb008008.
Dokka, R. K., G. F. Sella, and T. H. Dixon (2006), Tectonic control of subsidence and southward displacement of southeast Louisiana with respect to stable North America, *Geophys. Res. Lett.*, *33*, L23308, doi:10.1029/2006GL027250.
Dorale, J. A., B. P. Onac, J. J. Fornos, J. Gines, A. Gines, P. Tuccimei, and D. W. Peate (2010), Sea-level highstand 81,000 years ago in Mallorca, *Science*, *327*(5967), 860–863, doi:10.1126/science.1181725.
Dziewonski, A. M., and D. L. Anderson (1981), Preliminary reference Earth model, *Phys. Earth Planet. Int.*, *25*, 297–356.
Edrington, C. H., M. D. Blum, J. A. Nunn, and J. S. Hanor (2008), Long-term subsidence and compaction rates: A new model for the Michoud area, south Louisiana, *Gulf Coast Assoc. Geol. Soc. Trans.*, *58*, 261–272.
Fisk, H. N. (1939), Depositional terrace slopes in Louisiana, *J. Geomorphol.*, *2*, 181–200.
Fisk, H. N. (1944), Geological Investigation of the Alluvial Valley of the Lower Mississippi River, 78 pp., Mississippi River Commission, Vicksburg, Miss.
Fisk, H. N., and E. Jr.McFarlan (1955), Late Quaternary deltaic deposits of the Mississippi River, *Geol. Soc. Am. Spec. Pap.*, *62*, 279–302.
Frazier, D. E. (1967), Recent deltaic deposits of the Mississippi River: Their development and chronology, *Gulf Coast Assoc. Geol. Soc. Trans.*, *27*, 287–315.
González, J. L., and T. E. Törnqvist (2009), A new Late Holocene sea-level record from the Mississippi Delta: Evidence for a climate/sea level connection?, *Quat. Sci. Rev.*, *28*, 1737–1749, doi:10.1016/j.quascirev.2009.04.003.
Hutton, E. W. H., and J. P. M. Syvitski (2008), *Sedflux 2.0*: An advanced process-response model that generates three-dimensional stratigraphy, *Comput. Geosci.*, *34*, 1319–1337, doi:10.1016/j.cageo.2008.02.013.
Ivins, E. R., R. K. Dokka, and R. G. Blom (2007), Post-glacial sediment load and subsidence in coastal Louisiana, *Geophys. Res. Lett.*, *34*, L16303, doi:10.1029/2007GL030003.
Jurkowski, G., J. Ni, and L. Brown (1984), Modern uparching of the Gulf coastal plain, *J. Geophys. Res.*, *89*(B7), 6247–6255, doi:10.1029/JB089iB07p06247.
Karato, S.-I. (2008), *Deformation of Earth Materials: An Introduction to the Rheology of Solid Earth*, 463 pp., Cambridge Univ. Press, Cambridge, U. K.
Kendall, R. A., J. X. Mitroviva, and G. A. Milne (2005), On post-glacial sea level—II. Numerical formulation and comparative results on spherically symmetric models, *Geophys. J. Int.*, *161*, 679–706, doi:10.1111/j.1365-246X.2005.02553.x.
Kleman, J., K. Jansson, H. De Angelis, A. P. Stroeven, C. Hättestrand, G. Alm, and N. Glasser (2010), North American Ice Sheet build-up during the last glacial cycle, 115–21 kyr, *Quat. Sci. Rev.*, *29*, 2036–2051, doi:10.1016/j.quascirev.2010.04.021.
Klemann, V., and D. Wolf (1998), Modelling of stresses in the Fennoscandian lithosphere induced by Pleistocene glaciations, *Tectonophysics*, *294*, 291–303, doi:10.1016/S0040-1951(98)00107-3.
Kolb, C. R., and J. R. Van Lopik (1966), Depositional environments of the Mississippi River deltaic plain—Southeastern Louisiana, in *Deltas in Their Geologic Framework*, edited by M. L. Shirley, pp. 17–61, Houston Geological Society, Houston, Tex.
Kolker, A. S., M. A. Allison, and S. Hameed (2011), An evaluation of subsidence rates and sea-level variability in the northern Gulf of Mexico, *Geophys. Res. Lett.*, *38*, L21404, doi:10.1029/2011GL049458.
Kuecher, G. J., N. Chandra, H. H. Roberts, J. H. Suhayda, S. J. Williams, S. P. Penland, and W. J. Autin (1993), Consolidation settlement potential in south Louisiana, Proceedings, 8th Symposium on Coastal and Ocean Management, pp. 1197–1214, New Orleans, La.
Kulp, M., P. Howell, S. Adiau, S. Penland, J. Kindinger, and S. J. Williams (2002), Latest Quaternary stratigraphic framework of the Mississippi River delta region, *Gulf Coast Assoc. Geol. Soc. Trans.*, *52*, 573–582.
Kulp, M., D. Fitzgerald, and S. Penland (2005), Sand-rich lithosomes of the Holocene Mississippi River delta plain, in *River Deltas-Concepts, Models, and Examples, Society of Economic Mineralogists and Paleontologists Special Publication, no. 83*, edited by J. P. Bhattacharya and L. Giosan, pp. 277–291, Society for Sedimentary Geology, Tulsa, Okla.
Lambeck, K., and P. Johnston (1998), The viscosity of the mantle: Evidence from analyses of glacial-rebound phenomena, in *The Earth's Mantle: Composition, Structure, and Evolution Cambridge*, edited by I. Jackson, pp. 461–502, Cambridge Univ. Press, Cambridge, U.K.
Latychev, K., J. X. Mitrovica, J. Tromp, M. E. Tamisiea, D. Komatitsch, and C. C. Christara (2005), Glacial isostatic adjustment on 3-D Earth models: A finite volume formulation, *Geophys. J. Int.*, *161*, 421–444, doi:10.1111/j.1365-246X.2005.02536.x.
Ludwig, K. R., D. R. Muhs, K. R. Simmons, R. B. Halley, and E. A. Shinn (1996), Sea-level records at ~80 ka from tectonically stable platforms: Florida and Bermuda, *Geology*, *24*, 211–214, doi:10.1130/0091-7613(1996).
Mackin, J. H. (1948), Concept of the graded river, *Geol. Soc. Am. Bull.*, *59*, 463–511.
Manger, G. E (1963), Porosity and bulk density of sedimentary rocks, (U.S.) *Geol. Surv. Bull.* 1144-E URL: [Available at http://pubs.usgs.gov/bul/1144e/report.pdf.]
Meckel, T. A. (2008), An attempt to reconcile subsidence rates determined from various techniques in southern Louisiana, *Quat. Sci. Rev.*, *27*(15–16), 1517–1522, doi:10.1016/j.quascirev.2008.04.013.
Milne, G. A., and J. X. Mitrovica (1998), Postglacial sea-level change on a rotating Earth, *Geophys. J. Int.*, *133*, 1–19, doi:10.1046/j.1365-246X.1998.1331455.x.
Milne, G. A., and J. X. Mitrovica (2008), Searching for eustasy in deglacial sea-level histories, *Quat. Sci. Rev.*, *27*, 2292–2302, doi:10.1016/j.quascirev.2008.08.018.
Milne, G. A., and M. Peros (2013), Data-model comparison of Holocene sea-level change in the circum-Caribbean region, *Global Planet. Change*, *107*, 119–131, doi:10.1016/j.gloplacha.2013.04.014.
Milne, G. A., J. L. Davis, J. X. Mitrovica, H.-G. Scherneck, J. M. Johansson, M. Vermeer, and H. Koivula (2001), Space-geodetic constraints on glacial isostatic adjustment in Fennoscandia, *Science*, *291*, 2381–2385, doi:10.1126/science.1057022.
Mitrovica, J. X., J. Wahr, I. Matsuyama, and A. Paulson (2005), The rotational stability of an ice-age Earth, *Geophys. J. Int.*, *161*, 491–506, doi:10.1111/j.1365-246X.2005.02609.x.
Mitrovica, J. X. (1996), Haskell [1935] Revisited, *J. Geophys. Res.*, *101*, 555–569, doi:10.1029/95jb03208.
Mitrovica, J. X., and G. A. Milne (2002), On the origin of late Holocene highstands within equatorial ocean basins, *Quat. Sci. Rev.*, *21*, 2179–2190, doi:10.1016/S0277-3791(02)00080-X.
Mitrovica, J. X., and G. A. Milne (2003), On post-glacial sea level: I. General theory, *Geophys. J. Int.*, *154*, 253–267, doi:10.1046/j.1365-246X.2003.01942.x.
Morton, R. A., and J. C. Bernier (2010), Recent subsidence-rate reductions in the Mississippi Delta and their geological implications, *J. Coastal Res.*, *26*(3), 555–561, doi:10.2112/JCOASTRES-D-09-00014R1.1.
Murray, G. E. (1961), *Geology of the Atlantic and Gulf Coastal Provinces of North America*, 692 pp., Harper, New York.
Nittrouer, J. A., J. Shaw, M. P. Lamb, and D. Mohrig (2012), Spatial and temporal trends for water-flow velocity and bed-material sediment transport in the lower Mississippi River, *Geol. Soc. Am. Bull.*, *124*(3–4), 400–414, doi:10.1130/b30497.1.

Paulson, A., S. Zhong, and J. Wahr (2007), Limitations on the inversion for mantle viscosity from postglacial rebound, *Geophys. J. Intl.*, *168*, 1195–1209, doi:10.1111/j.1365-246X.2006.03222.x.

Peltier, W. R. (1974), The impulse response of a Maxwell Earth, *Rev. Geophys.*, *12*(4), 649–669, doi:10.1029/RG012i004p00649.

Peltier, W. R. (2004), Global glacial isostasy and the surface of the ice-age earth: The ICE-5G (VM2) model and GRACE, *Annu. Rev. Earth Planet. Sci.*, *32*, 111–49, doi:10.1146/annurev.earth.32.082503.144359.

Peltier, W. R. (1996), Mantle viscosity and ice-age ice sheet topography, *Science*, *273*, 1359–1364, doi:10.1126/science.273.5280.1359.

Penland, S., and K. E. Ramsey (1990), Relative sea-level rise in Louisiana and the Gulf of Mexico: 1908–1988, *J. Coastal Res.*, *6*, 323–342.

Potter, E.-K., and K. Lambeck (2003), Reconciliation of sea-level observations in the Western North Atlantic during the last glacial cycle, *Earth Planet. Sci. Lett.*, *217*(1–2), 171–181, doi:10.1016/s0012-821x(03)00587-9.

Ritsema, J., A. Deuss, H. J. van Heijst, and J. H. Woodhouse (2011), S40RTS: A degree-40 shear-velocity model for the mantle from new Rayleigh wave dispersion, teleseismic traveltime and normal-mode splitting function measurements, *Geophys. J. Intl.*, *184*, 1223–1236, doi:10.1111/j.1365-246X.2010.04884.x.

Rittenour, T. M., M. D. Blum, and R. J. Goble (2007), Fluvial evolution of the lower Mississippi River valley during the last 100 k.y. glacial cycle: Response to glaciation and sea-level change, *Geol. Soc. Am. Bull.*, *119*(5–6), 586–608, doi:10.1130/b25934.1.

Saucier, R. T. (1994), *Geomorphology and Quaternary Geologic History of the Lower Mississippi Valley*, 364 pp., Mississippi River Commission, Vicksburg.

Schumm, S. A., J. F. Dumont, and J. M. Holbrook (2002), *Active Tectonics and Alluvial Rivers*, 292 pp., Cambridge Univ. Press, Cambridge, U. K.

Shen, Z., T. E. Törnqvist, W. J. Autin, Z. R. P. Mateo, K. M. Straub, and B. Mauz (2012), Rapid and widespread response of the Lower Mississippi River to eustatic forcing during the last glacial-interglacial cycle, *Geol. Soc. Am. Bull.*, *124*(5–6), 690–704, doi:10.1130/b30449.1.

Simms, A. R., K. Lambeck, A. Purcell, J. B. Anderson, and A. B. Rodriguez (2007), Sea-level history of the Gulf of Mexico since the Last Glacial Maximum with implications for the melting history of the Laurentide Ice Sheet, *Quat. Sci. Rev.*, *26*, 920–940, doi:10.1016/j.quascirev.2007.01.001.

Simms, A. R., J. B. Anderson, R. DeWitt, K. Lambeck, and A. Purcell (2013), Quantifying rates of coastal subsidence since the last interglacial and the role of sediment loading, *Global Planet. Change*, *111*, 296–308.

Snow, R. S., and R. L. Slingerland (1987), Mathematical modeling of graded river profiles, *J. Geol.*, *95*, 15–33, doi:10.1086/629104.

Stanley, D. J., A. G. Warne, and J. B. Dunbar (1996), Eastern Mississippi delta: Late Wisconsin unconformity, overlying transgressive facies, sea level and subsidence, *Eng. Geol.*, *45*, 359–381.

Stelting, C. E., L. Droz, A. H. Bouma, J. M. Coleman, M. Cremer, A. W. Meyer, W. R. Normark, S. O'Connell, and D. A. V. Stow (1986), Late Pleistocene seismic stratigraphy of the Mississippi Fan, in *Initial reports of the deep sea drilling project 96*, edited by A. H. Bouma, et al., pp. 437–456, U.S. Govt. Printing Office, Washington, D. C.

Stokes, C. R., L. Tarasov, and A. S. Dyke (2012), Dynamics of the North American Ice Sheet Complex during its inception and build-up to the Last Glacial Maximum, *Quat. Sci. Rev.*, *50*, 86–104, doi:10.1016/j.quascirev.2012.07.009.

St-Onge, D. A. (1987), The Sangamonian Stage and the Laurentide Ice Sheet, *Geogr. Phys. Quat.*, *41*, 189–198.

Straub, K. M., C. Paola, D. Mohrig, M. A. Wolinsky, and T. George (2009), Compensational stacking of channelized sedimentary deposits, *J. Sediment. Res.*, *79*, 673–688, doi:10.2110/jsr.2009.070.

Syvitski, J. (2008), Deltas at risk, *Sustain. Sci.*, *3*(1), 23–32, doi:10.1007/s11625-008-0043-3.

Tesauro, M., P. Audet, M. K. Kaban, R. Bürgmann, and S. Cloetingh (2012), The effective elastic thickness of the continental lithosphere: Comparison between rheological and inverse approaches, *Geochem. Geophys. Geosyst.*, *13*, Q09001, doi:10.1029/2012GC004162.

Törnqvist, T. E., J. L. González, L. A. Newsom, K. van der Borg, A. F. M. de Jong, and C. W. Kurnik (2004), Deciphering Holocene sea-level history on the U.S. Gulf Coast: A high-resolution record from the Mississippi Delta, *Geol. Soc. Am. Bull.*, *116*, 1026–1039, doi:10.1130/b2525478.1.

Törnqvist, T. E., S. J. Bick, K. van der Borg, and A. F. M. de Jong (2006), How stable is the Mississippi Delta?, *Geology*, *34*(8), 697–700, doi:10.1130/G22624.1.

Törnqvist, T. E., D. J. Wallace, J. E. A. Storms, J. Wallinga, R. L. van Dam, M. Blaauw, M. S. Derksen, C. J. W. Klerks, C. Meijneken, and E. M. A. Snijders (2008), Mississippi Delta subsidence primarily caused by compaction of Holocene strata, *Nat. Geosci.*, *1*(3), 173–176, doi:10.1038/ngeo129.

Vincent, J.-S., and V. K. Prest (1987), The Early Wisconsinan History of the Laurentide Ice Sheet, *Geogr. Phys. Quat.*, *41*, 199–213.

Wang, H., L. Xiang, L. Jia, L. Jiang, Z. Wang, B. Hu, and P. Gao (2012), Load Love numbers and Green's functions for elastic Earth models PREM, iasp91, ak135, and modified models with refined crustal structure from Crust 2.0, *Comput. Geosci.*, *49*, 190–199, doi:10.1016/j.cageo.2012.06.022.

Watts, A. B., S. J. Zhong, and J. Hunter (2013), The behavior of the lithosphere on seismic to geologic timescales, *Annu. Rev. Earth Planet. Sci.*, *41*, 443–68, doi:10.1146/annurev-earth-042711-105457.

Watts, T. (2001), *Isostasy and Flexure of the Lithosphere*, pp. 1–451, Cambridge Univ. Press, Cambridge, U.K.

Wehmiller, J. F., K. R. Simmons, H. Cheng, R. L. Edwards, J. Martin-McNaughton, L. L. York, D. E. Krantz, and C. C. Shen (2004), Uranium-series coral ages from the U.S. Atlantic Coastal Plain—The "80 ka problem" revisited, *Quat. Int.*, *120*, 3–14, doi:10.1016/j.quaint.2004.01.002.

Whitehouse, P., K. Latychev, G. A. Milne, J. X. Mitrovica, and R. Kendall (2006), Impact of 3-D Earth structure on Fennoscandian glacial isostatic adjustment: Implications for space-geodetic estimates of present-day crustal deformations, *Geophys. Res. Lett.*, *33*, L13502, doi:10.1029/2006GL026568.

Woodbury, H. O., I. B. Jr.Murray, P. J. Pickford, and W. H. Akers (1973), Pliocene and Pleistocene depocenters, outer continental shelf, Louisiana and Texas, *Am. Assoc. Peter. Geol. B.*, *57*, 2428–2439.

Wu, X., X. Collilieux, Z. Altamimi, B. L. A. Vermeersen, R. S. Gross, and I. Fukumori (2011), Accuracy of the International Terrestrial Reference Frame origin and Earth expansion, *Geophys. Res. Lett.*, *38*, L13304, doi:10.1029/2011gl047450.

Yu, S.-Y., T. E. Törnqvist, and P. Hu (2012), Quantifying Holocene lithospheric subsidence rates underneath the Mississippi Delta, *Earth Planet. Sci. Lett.*, *331–332*, 21–30, doi:10.1016/j.epsl.2012.02.021.